AD-A097 941 SCIENCE APPLICATIONS INC PALO ALTO CALIF F/G 20/8
PROPAGATION OF LOW-GAMMA ION BEAMS -- THE RESISTIVE HOSE INSTAB--ETC(U)
DEC 80 R L FEINSTEIN N00014-79-C-0221
UNCLASSIFIED SAI-1-227-00-413-00 NL

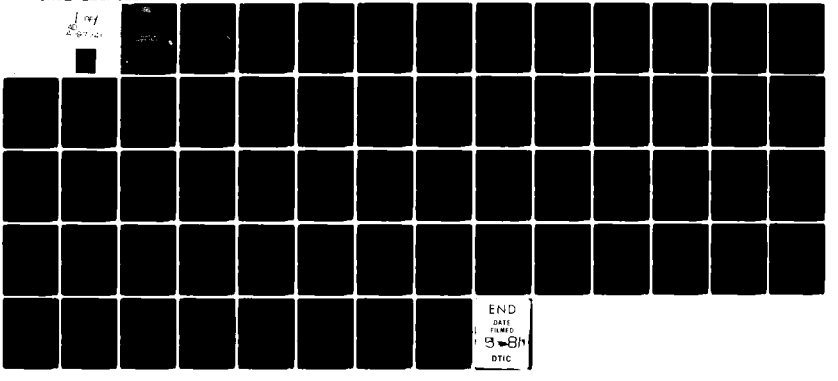

END
DATE FILMED
9-81
DTIC

LEVEL II

AD A097941

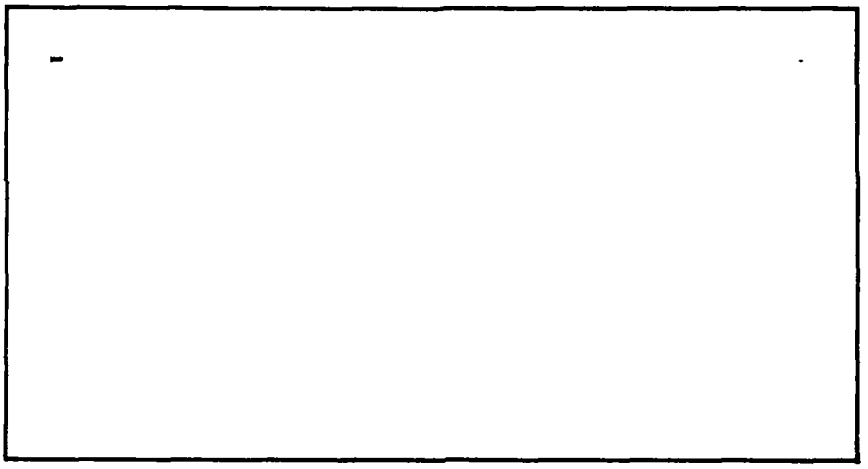

science applications inc.

PALO ALTO

81 2 04 069

(14) SAI-1-227-00-413-00

(1)

PROPAGATION OF LOW-GAMMA ION BEAMS -- THE RESISTIVE HOSE INSTABILITY

(12) 62

(11) 30 December 1980

(10) Prepared by
R. Leon Feinstein

for the

(15) Office of Naval Research
~~Contract No.~~ N00014-79-C-0221
Modification P00002

SCIENCE APPLICATIONS, INC • 5 PALO ALTO SQUARE, SUITE 200, PALO ALTO, CA 94304
ALBUQUERQUE • ANN ARBOR • ARLINGTON • BOSTON • CHICAGO • HUNTSVILLE • LA JOLLA
LOS ANGELES • ROCKVILLE • SUNNYVALE • TUCSON

TABLE OF CONTENTS

I. INTRODUCTION

Ion beams have attracted considerable interest in recent years as a result of their potential application as drivers for inertial confinement fusion. Due to the state-of-the-art of accelerator technology, however, theoretical advances in beam propagation have focused on the properties of high-energy (high-gamma) electron beams. Some important simplifying assumptions are made for highly relativistic beams which do not apply at low-gamma. In past studies (Refs. 1 and 2), we began to relax these model assumptions to address the axi-symmetric evolution of ion beams. In this ~~SAI final~~ report on the propagation of low-gamma ion beams, we explore the resistive hose instability with longitudinal velocity-spread.

For energies of interest, the theoretical models of electron beam propagation cannot be directly applied to ions because of their low relativistic gamma (γ) factors. For example, for kinetic energy equal to 50 MeV, $\gamma \simeq 99$. for electrons compared to $\gamma \simeq 1.05$ for protons. If the beam propagates in the longitudinal direction (along the z-axis), the effective inertial mass of the beam particles in the z-direction is given approximately by $\gamma^3 m$, where m is the particle rest mass. This suggests that light ions are considerably more susceptible to longitudinal acceleration than electrons of equivalent kinetic energy; the longitudinal particle-motion cannot be ignored as in the electron case. This adds a new dimension to ion beam propagation.

The consequences of the longitudinal motion on beam stability can be divided into three categories:

(1) Longitudinal spreading of the beam pulse due to longitudinal velocity-spread (longitudinal temperature);

(2) Longitudinal mass (bunching) instability; and

(3) Resistive hose instability with longitudinal velocity-spread.

Categories (1) and (2) are unique to light-ion propagation, while (3) requires modification to existing electron-beam hose stability theory.

In order to address issue (1) above, we developed the low-γ propagation code LOGAP (Ref. 1) which models the axi-symmetric (monopole) evolution of a single pulse (with longitudinal and transverse degrees of freedom). LOGAP consists of four basic components: electromagnetic field algorithm GEM, which generates both longitudinal and radial field profiles in real-time; the highly-developed, chemistry package BMCOND, which generates the conductivity profiles in the ambient gas resulting from the passage of the beam (Ref. 3); the HIGAP algorithm for solving the radial-envelope equation of motion (Ref. 3 and 4); and the longitudinal dispersion algorithm LNGDSP which describes the longitudinal flow of beam particles via a fluid model. A detailed discussion of LOGAP is found in References 1 and 2; for completeness, however, we provide in Appendix A excerpts from Reference 1 describing both GEM and LNGDSP. A stability analysis of the GEM field algorithm is given in Reference 2 and is reproduced here in Appendix B.

Longitudinal spreading of the beam pulse is a concern since it could transform a given pulse into a longer one with lower current which would then be less hose-stable. It has been suggested (Ref. 5) that the spreading might be contained by the self-induced longitudinal electric field at the front and rear of the pulse, keeping the beam particles trapped inside. Preliminary results from LOGAP to date have failed to verify the existence of this self-trapped mode.

It should be emphasized that in LOGAP longitudinal and transverse degrees of freedom are essentially decoupled. If we partition the beam particles into subgroups according to their v_z-velocity, then LOGAP assumes that the current-density of all subsets, regardless of v_z, have the same radial profile. A more realistic approach would be to allow the different subsets to expand radially at different rates; the low-velocity subgroups would expand faster since their particle radial-motion is confined by a relatively

weaker magnetic pinch force. The very low velocity particles (which in LOGAP contribute to the longitudinal spreading of the pulse tail) may "evaporate" in the radial direction. Therefore, LOGAP should be appropriately modified to account for transverse evaporation for a definitive test of the self-trapped pulse mode.

The longitudinal bunching instability has been examined by Sloan *et. al.* (Ref. 6) and is found to be Landau damped when the longitudinal rms velocity spread is greater than some minimum value [see Eq. (104) below]. For a (50 MeV, 10 ka) proton beam, this minimum vales is $\sim.075\ v_o$, where v_o is the mean velocity of beam particles. This should be well satisfied at the exit-port of an Auto-Resonant Accelerator (ARA), for example [see Eq. (101) below]; if not, the bunching instability itself and/or the self-induced electric field will probably ensure that the rms velocity-spread within the pulse is more than enough to stabilize it.

In the remainder of this report, we examine the effects of longitudinal velocity-spread on the resistive hose instability. The rigid beam model and the multi-disk, distributed-mass model of Lee (Ref. 7) are both modified to account for the phase-mixing associated with the distribution of longitudinal velocities. Beam particles are partitioned into subgroups according to their v_z-velocity with each subset experiencing an independent transverse displacement. The resulting equations of motion are solved for mode growth in the context of an initial-value problem with finite pulse length. Upper-bounds in hose-mode growth are found via saddle-point analysis as well as conditions for "absolute" hose stability.

The results of this preliminary study suggest that the light-ion, low-γ beam may have a hose stability advantage over a comparable electron beam. For example, the (50 MeV, 10 ka) proton beam with longitudinal rms velocity-spread of $\sim.1\ v_o$ has an estimated hose-stable pulse length that is nearly twice the zero-spread model prediction. With an rms spread of $.26\ v_o$, it approaches an "absolute" hose-stable regime; but, if the pulse spreads longitudinally (i.e., no self-trapping), the beam current decreases until hose-growth recovers.

The analysis in this report is semi-quantitative in that it is based on a single-mode approach with various simplifying assumptions: the conductivity channel is assumed fixed in space independent of beam evolution; the plasma return currents have a prescribed radial-profile; and the longitudinal and transverse equations of motion are decoupled. In a comprehensive treatment, these assumptions should be relaxed and the equations of motion solved numerically.

In Section II, the basic particle and electromagnetic field equations are presented. The equilibrium state is described in Section III with emphasis on the isothermal Bennett distribution and the longitudinal velocity distribution. Hose-like perturbations are considered in Section IV; the rigid-beam dispersion equation with longitudinal velocity-spread is derived in Section IV.A.; and the modified distributed-mass model and the single-mode dispersion equation is derived in Section IV.B. The dispersion equations are analyzed in Sections V.A. and V.B., respectively. And in Section VI, we interpret the results in the context of the ARA and longitudinal mass instability.

II. PARTICLE AND FIELD EQUATIONS

We consider a beam of ions with mass m and charge $Z_b e$ propagating with a mean velocity v_o in the positive z-direction through an ionized gas. The ambient gas-plasma is characterized in the present study by a real, scalar conductivity σ which is assumed to be known and independent of beam perturbations. In practice, the σ-channel could be strongly affected by the passage of the beam through the gas via direct collisional ionization and electromagnetic field breakdown, but these effects are neglected here.

The beam current I_b is assumed to be small compared to the Alfvén current (I_A):

$$I_b << I_A \equiv \gamma_o \beta_o \frac{4\pi mc^2}{eZ_b R_o} = \gamma_o \beta_o \left(\frac{m}{m_e}\right) \frac{1}{Z_b} (17 \text{ ka}) \tag{1}$$

where $\gamma_o = (1 - \beta_o^2)^{-1/2}$ is the relativistic factor for the mean velocity $v_o = \beta_o c$, m_e is the electron mass and R_o is the resistance of free space ($R_o = 376.73$ ohm). Thus, the paraxial approximation is adopted, i.e.,

$$|p_\perp| << p_o = \gamma_o m v_o \tag{2}$$

where $|p_\perp|$ refers to the amplitude of the single-particle transverse momentum.

We also assume that σ is large enough that charge-neutralization time is small compared to the magnetic decay time, and hence, the displacement current can be neglected. Together with the paraxial assumption (2), this allows a reduction of Ampere's law to the form

$$\nabla_\perp^2 A_z - \frac{R_o \sigma}{c} \frac{\partial A_z}{\partial t} = -J_{bz} \tag{3}$$

where the electromagnetic fields are adequately described by the longitudinal component of the magnetic potential A_z:

$$\vec{H}_\perp = \vec{\nabla}_\perp \times (A_z \hat{e}_z) \tag{4}$$

$$E_z = -\frac{R_o}{c}\frac{\partial A_z}{\partial t} \tag{5}$$

The transverse components (x,y) are denoted by the symbol ($\perp$), and J_{bz} is the beam current-density in the z-direction.

A particular beam particle with velocity $\vec{v} = (\vec{v}_\perp, v_z)$ satisfies the equations of motion

$$\frac{dp_z}{dt} = -\frac{eZ_b R_o}{c}\left[\frac{\partial A_z}{\partial t} + (\vec{v}_\perp \cdot \vec{\nabla}_\perp) A_z\right] \tag{6}$$

$$\frac{d\vec{p}_\perp}{dt} = \frac{eZ_b R_o}{c} v_z \vec{\nabla}_\perp A_z \tag{7}$$

By the paraxial assumption (2), we ignore the variations in p_z and assume that v_z and the relativistic factors $\gamma = [1 - (v_z^2/c^2) - (v_\perp^2/c^2)]^{1/2}$ are constant for each particle orbit, i.e.,

$$\frac{dp_z}{dt} = \frac{d}{dt}(\gamma m v_z) = 0 \tag{8}$$

The mean particle momentum is expressed by

$$\langle p_z \rangle \equiv p_o = \gamma_o m v_o \tag{9}$$

where the bracket $\langle\ \rangle$ denotes the instantaneous average over all beam particles in a disk at (z,t). However, it is also assumed that p_o be independent of (z,t) over the time scales of interest. The energy of a particle with $v_z = v_o$ is given by

$$E_o = \gamma_o m c^2 \tag{10}$$

It is convenient to express the particle energy and momentum in terms of the momentum variable q and velocity spread ν where

$$q \equiv p_z - p_o = \gamma m v_z - \gamma_o m v_o \tag{11}$$

$$\nu \equiv v_z - v_o \tag{12}$$

with $q << p_o$. By (8), both q and ν are considered constants of motion. To order $q^2/(\gamma_o^2 m^2 c^2)$, we have

$$E \equiv \gamma mc^2 \simeq \gamma_o mc^2 + \frac{p_o q}{\gamma_o m} + \frac{q^2}{2\gamma_o^3 m} + \frac{p_\perp^2}{2\gamma_o m} \tag{13}$$

$$\vec{p}_\perp \simeq \gamma_o m \vec{v}_\perp \tag{14}$$

Expanding (11) about v_o, it is easily shown that

$$q \simeq \gamma_o^3 m \nu \tag{15}$$

It follows that approximation (8) is valid so long as

$$\frac{|v_\perp|}{\gamma_o^3} << \frac{v_o}{\gamma_o} \tag{16}$$

Hence, the transverse single particle equation of motion (7) can be approximated to lowest order by

$$\frac{d^2\vec{r}_\perp}{dt^2} = \frac{eZ_b R_o}{\gamma_o mc} v_o \vec{\nabla}_\perp A_z \tag{17}$$

Note that the r.h.s. of Eq. (17) is independent of ν. This allows us to treat particles with different v_z by the same pinch-potential. In subsequent sections, beam particles are divided into subgroups according to their longitudinal v_z velocity. Eq. (17) implies that all subsets, regardless of v_z, have the same equilibrium radial-profile.

For closure, we need the distribution function $f(\vec{r},z,\vec{v}_\perp, v_z,t)d^3r\, d^3v$ which represents the number of beam ions in the phase-space volume $d^2r_\perp\, dz\, d^2v_\perp\, dv_z$. The beam current density is then defined by

$$J_{bz} = eZ_b \int d^2v_\perp \int dv_z\, v_z\, f = eZ_b v_o n \tag{18}$$

where n is the beam-particle density. From continuity and Eqs. (7) and (8), f satisfies the Vlasov equation

$$\frac{\partial f}{\partial t} + \vec{v}_\perp \cdot \vec{\nabla}_\perp f + v_z \frac{\partial f}{\partial z} + \frac{eZ_b R_o v_z}{c} \vec{\nabla}_\perp A_z \cdot \vec{\nabla}_{p\perp} f = 0 \tag{19}$$

It is useful to introduce the variable ξ defined by

$$\xi \equiv v_o t - z \tag{20}$$

and replace the independent variables (z,t) by (ξ,z) in all the relevant equations. The derivatives transform as follows:

$$\frac{\partial}{\partial z} \Rightarrow \frac{\partial}{\partial z} - \frac{\partial}{\partial \xi} \tag{21a}$$

$$\frac{\partial}{\partial t} \Rightarrow v_o \frac{\partial}{\partial \xi} \tag{21b}$$

$$\frac{d}{dt} \equiv \frac{\partial}{\partial t} + v_z \frac{\partial}{\partial z} \Rightarrow v_o \frac{d}{dz} \equiv v_z \frac{\partial}{\partial z} - \nu \frac{\partial}{\partial \xi} \tag{21c}$$

Employing (20) and (21) in Eqs. (3), (17), and (19), we arrive at our final set of model equations (dropping subscript z from now on)

$$\vec{\nabla}_\perp^2 A - \frac{R_o \sigma v_o}{c} \frac{\partial A}{\partial \xi} = -J_b \tag{22}$$

$$\frac{d^2}{dz^2} \vec{r}_\perp = \frac{eZ_b R_o}{\gamma_o m c v_o} \vec{\nabla}_\perp A \tag{23}$$

$$J_b = eZ_b \int d\hat{a}\, v_\perp \int dv\; v\; f \tag{24}$$

$$v_o \frac{df}{dz} + \vec{v}_\perp \cdot \vec{\nabla}_\perp f + \frac{eZ_b R_o v_o}{c} \vec{\nabla}_\perp A \cdot \vec{\nabla}_{p_\perp} f = 0 \tag{25}$$

These are employed in the following sections to treat the resistive hose instability. We begin by exploring the axi-symmetric equilibrium state.

III. EQUILIBRIUM

Our equilibrium beam is assumed to be cylindrically symmetric about the z-axis. Adopting cylindrical coordinates (r,θ,z), the single particle equation (23) becomes

$$\frac{d^2\vec{r}}{dz^2} = -k_\beta^2 \vec{r} \tag{26}$$

$$k_\beta^2 (r) \equiv - \frac{eZ_b R_o \beta_o}{\gamma_o m v_o^2} \frac{1}{r} \frac{dA_o}{dr} \tag{27}$$

where k_β is the betatron frequency and A_o refers to the equilibrium potential which by (22) and (24) satisfies

$$\frac{1}{r} \frac{d}{dr} r \frac{dA_o}{dr} = -J_{bo} + \frac{R_o \sigma v_o}{c} \frac{\partial A_o}{\partial \xi} \simeq -(1 - \delta_m) J_{bo} \tag{28}$$

$$J_{bo} = eZ_b \int d^2 v_\perp \int dv \; v \; f_o \tag{29}$$

In (28) we have assumed that the plasma return current-density is represented by $-\delta_m J_{bo}$, where the current neutralization factor δ_m is assumed to be a constant. This is a reasonable approximation when $\delta_m \lesssim .5$. For $\delta_m \gtrsim .5$, since the return current density has a radial profile considerably different from J_{bo}, the r.h.s. of (28) is not valid.

Since the equilibrium distribution function f_o is an integral of motion, it can be written as a function of the constants of motion. We choose the separable form

$$f_o = G_\perp(w) \; F(\nu) \tag{30}$$

where

$$w \equiv v_\perp^2 - \frac{2eZ_b R_o \beta_o}{\gamma_o m v_o^2} A_o \tag{31}$$

is a constant of motion according to Eq. (26) and the velocity spread ν is assumed constant by our model assumption (8). G and F are normalized

such that

$$n_o(r) = \int d^2 v_\perp \, G_\perp \tag{32}$$

$$1 = \int dv \, F \tag{33}$$

where n_o is the equilibrium particle density.

For the Maxwellian distribution, G and F take the form

$$G_M = \frac{\hat{n}_o}{\pi u_\perp^2} \, e^{-(w/u_\perp^2)} \tag{34}$$

$$F_M = \frac{1}{\sqrt{2\pi}\, u} \, e^{-(v^2/2u^2)} \tag{35}$$

where the mean-square velocities are defined by

$$u_\perp^2 \equiv \langle v_\perp^2 \rangle \tag{36}$$

$$u^2 \equiv \langle v^2 \rangle \tag{37}$$

The normalization constraints (32) and (33) are appropriately satisfied. The transverse distribution G_M is the important isothermal case described by Bennett (Ref. 8). It has been shown by Lee et. al. (Refs. 4 and 9) that the Bennett distribution is a good approximation to the pinch-equilibrium state.

It can be readily verified that the Bennett profile

$$J_{bo} = J_B \equiv \frac{I_b}{\pi a^2} \, \frac{1}{(1 - r^2/a^2)^2} \tag{38}$$

and the magnetic potential

$$A_o = A_B = - \frac{(1 - \delta_m) \, I_b}{4\pi} \, \ell n \, (1 + r^2/a^2) \tag{39}$$

satisfy Eqs. (28), (29), (31), and (34), with

$$I_b = eZ_b \hat{n}_o v_o \pi a^2 \tag{40}$$

Taking the virial moment of (26), the mean-square transverse velocity satisfies the equilibrium condition

$$\frac{u_\perp^2}{v_o^2} \equiv \frac{\langle v_\perp^2 \rangle}{v_o^2} = \langle k_\beta^2 r^2 \rangle = (1 - \delta_m) \frac{I_b}{I_A} \tag{41}$$

with the Alfvén current I_A defined by (1). This velocity-spread is due entirely to betatron oscillations -- energy-spread effects are neglected.

For later reference, we express the longitudinal mean-square velocity spread u^2 in terms of the energy spread $\Delta E = (\gamma - \gamma_o)mc^2$. From Eqs. (13) through (15), we derive the relation

$$\frac{u^2}{v_o^2} \equiv \frac{\langle v^2 \rangle}{v_o^2} \simeq \frac{1}{(\gamma_o^2 - 1)^2} \frac{\langle (\Delta E)^2 \rangle}{E_o^2} \tag{42}$$

$$E_o \equiv \gamma_o mc^2 \tag{43}$$

Note that if we attribute the longitudinal velocity-spread to betatron motion only--i.e., ignoring energy-spread--then

$$\left(\frac{u^2}{v_o^2} \right)_{\text{betatron}} = \frac{u_\perp^2}{2\gamma_o^2 v_o^2} = \frac{(1 - \delta_m)}{2\gamma_o^2} \frac{I_b}{I_A} \tag{44}$$

which places a lower bound on the longitudinal temperature.

As a consequence of ignoring the ν-dependence in $k_\beta(r)$, Eq. (27), the radial profile of the equilibrium current is independent of the particular subset of beam particles with the same ν. This is expressed explicitly by introducing the partial current-density $\hat{J}_{bo}(r,\nu)$ for the subset of particles

with longitudinal velocity $v = v_o + \nu$: i.e.,

$$\hat{J}_{bo}(r,\nu) = F(\nu)\, J_{bo}(r) \tag{45}$$

$$J_{bo}(r) = \int d\nu\, \hat{J}_{bo}(r,\nu) \tag{46}$$

In subsequent sections, we shall treat each subset of particles separately in order to account for the longitudinal velocity effects on hose.

IV. HOSE DISPERSION EQUATIONS

Hose instability is treated by considering small amplitude perturbations of the form

$$\delta J_b = J_b - J_{bo} = J_{b1}\, e^{i\theta} \tag{47a}$$

$$\delta \hat{J}_b(\nu) = \hat{J}_b(\nu) - \hat{J}_{bo}(\nu) = \hat{J}_{b1}(\nu)\, e^{i\theta} \tag{47b}$$

$$\delta A = A - A_o = A_1\, e^{i\theta} \tag{47c}$$

$$\delta f = f - f_o = f_1\, e^{i\theta} \tag{47d}$$

where the zero subscript refers to the axi-symmetric equilibrium state discussed in the last section. $\hat{J}_b(r,\theta,z,\nu)d\nu$ represents the partial current-density of beam particles with longitudinal velocity between $(v_o + \nu)$ and $(v_o + \nu + d\nu)$. The perturbed amplitudes $(\hat{J}_{b1}, A_1, f_1)$ are assumed to be small. Note that the azimuthal dependence $e^{i\theta}$ in (47) is selected specifically for the hose mode.

In this present study, we consider the longitudinal velocity-spread effects in the contexts of two models: the rigid-beam and field model; and the multi-disk distributed-mass model of Reference 7.

IV.A. Rigid-Beam and Field Model

Following the rigid-beam development of Reference 7 , we represent the perturbed, partial current-density $\hat{J}_{b1}$ to lowest order by

$$\hat{J}_{b1} = -\hat{X}_\nu(\xi,z)\,\frac{d\hat{J}_{bo}}{dr} \tag{48}$$

An equation of motion for the transverse displacement amplitude $\hat{X}_\nu$ can be derived by averaging Eq. (23) over all particles in the disk (ξ,z) with v $(= v_o + \nu)$. Employing the rigid-field assumption,

$$A_1(\xi) = -\,D(\xi)\,\frac{dA_o}{dr} \tag{49}$$

we find

$$\frac{d^2\hat{X}_\nu}{dz^2} \simeq \frac{eZ_bR_o\pi}{\gamma_o mcv_o I_b}\,[D(\xi) - \hat{X}_\nu(\xi,z)](1-\delta_m)\int_0^\infty rdr\,(J_{bo})^2 \tag{50}$$

With the Bennett profile $J_{bo} = J_B$, Eq. (38), (50) simplifies to

$$\frac{d^2\hat{X}_\nu}{dz^2} \simeq k_{sB}^2\,[D(\xi) - \hat{X}_\nu(\xi,z)] \tag{51}$$

with

$$k_{sB}^2 \equiv (1-\delta_m)\,I_b\,\frac{eZ_bR_o}{6\pi a^2\gamma_o mcv_o} \tag{52}$$

$$= \frac{2}{3}\,\frac{(1-\delta_m)}{a^2}\,\frac{I_b}{I_A} \tag{53}$$

The perturbed form of Ampere's law (22) is

$$\frac{d}{dr}\left(\frac{1}{r}\frac{d}{dr}\, r\, A_1\right) - \frac{R_o \sigma v_o}{c}\,\frac{\partial A_1}{\partial \xi} = -J_{b1} = -\int d\nu\, \hat{J}_{b1} \tag{54}$$

Substituting the rigid-beam and field representations (48) and (49) into (54), multiplying by dA_0/dr, and integrating over the radius, we find the simple relation

$$D(\xi) + \tau_1 \frac{\partial D(\xi)}{\partial \xi} = \frac{\langle X(\xi,z)\rangle}{1 - \delta_m} \tag{55}$$

where

$$\langle X(\xi,z)\rangle = \int d\nu\, F(\nu)\, \hat{X}_\nu(\xi,z) \tag{56}$$

For the Bennett equilibrium, the dipole magnetic-decay length τ_1 is defined by

$$\tau_1 \equiv \frac{3R_o\beta_o}{2\,a^2}\int_0^\infty r\, dr\;\; \sigma(r)\,\frac{r^2}{(1 + r^2/a^2)^2} \tag{57}$$

For,

$$\sigma(r) = \sigma_o\;\frac{1}{(1 + r^2/a^2)^2} \tag{58}$$

we have

$$\tau_1 = \frac{R_o \sigma_o a^2 \beta_o}{8} \tag{59}$$

Equations (51), (55), and (56) specify completely the generalization of the rigid-beam model for longitudinal velocity-spread. It differs from the zero temperature model (Ref. 7) by the full z-derivative in (51) and the v - average (56).

If initial conditions are imposed at $z = 0$ for $\xi \gtrsim 0$ (where the pulse head begins at $\xi = 0$), then a Laplace transform analysis of Eqs. (51) and (55) results in growth for the displacement $\langle X\rangle$ bounded by

$$\langle X \rangle \propto \frac{1}{2\pi} \int_{-\infty + i\varepsilon}^{+\infty + i\varepsilon} d\Omega_o \, H(\Omega_o) \, e^{g(\Omega_o, \xi, z)} \tag{60a}$$

where $H(\Omega_o)$ depends on the initial perturbation of the pulse. The growth-phase exponent g is expressed by

$$g = -i \frac{\Omega_o}{v_o} z - i \frac{\omega(\Omega_o)}{v_o} \xi \tag{60b}$$

where $\omega(\Omega_o)$ is extracted from the single-mode dispersion equation derived below. Note that the contour of integration lies in the upper (Im $\Omega_o > 0$) half-plane.

In a single-mode approach, we assume

$$D, X_\nu, \langle X \rangle \propto e^{-i(kz - \omega t)} \tag{61a}$$

Transforming to the independent variables (ξ, z), Eq. (20), we have

$$D, X_\nu, \langle X \rangle \propto e^{-i[(\Omega_o/v_o)z + (\omega/v_o)\xi]} \tag{61b}$$

where
$$\Omega_o \equiv \omega - k v_o \tag{61c}$$

Substituting (61) into Eqs. (51) and (55), employing the z-derivative (21c), we arrive at the rigid-beam dispersion equation

$$-i\omega(\Omega_o)\lambda = \frac{1}{(1 - \delta_m)} \int d\nu \, \frac{F(\nu)}{[1-(\Omega_o - k\nu)^2]} - 1 \tag{62}$$

where we have transformed to the dimensionless units

$$\frac{\Omega_o}{v_o k_{sB}} \Rightarrow \Omega_o \, , \quad \frac{k}{k_{sB}} \Rightarrow k \tag{63a}$$

$$\frac{\omega}{v_o k_{sB}} \Rightarrow \omega \quad , \qquad \tau_1 k_{sB} \equiv \lambda \tag{63b}$$

$$\frac{\nu}{v_o} = \nu \quad , \quad \frac{u}{v_o} \Rightarrow u \tag{63c}$$

We now consider various specific forms for the distribution $F(\nu)$.

We recover the cold fluid (or zero temperature) results of Reference 7 by choosing

$$F_c(\nu) = \delta(\nu) \tag{64}$$

With this distribution, (62) becomes

$$-i\omega(\Omega_o)\lambda = \frac{1}{(1 - f_m)[1 - \Omega_o^2]} - 1 \tag{65}$$

which agrees with the usual form of the rigid-beam dispersion relation -- with the exception of the current-neutralization factor in the denominator which is usually set equal to zero.

For finite temperature hose, the Lorentzian distribution

$$F_L(\nu) = \frac{\Delta}{\pi} \frac{1}{\nu^2 + \Delta^2} \tag{66}$$

is particularly convenient since the integral in (62) can be performed analytically. Any function $K(\nu)$ which is analytic in the lower half-plant (Im ν < o) with peak amplitude less than $|\nu|^2$ satisfies the relation

$$\int_{-\infty}^{+\infty} d\nu \, F_L(\nu) \, K(\nu) = K(\nu = -i\Delta) \tag{67}$$

Hence, (62) becomes

$$-i\omega(\Omega_o)\lambda = \frac{1}{(1 - \delta_m)[1 - (\Omega_o + ik\Delta)^2]} - 1 \qquad (68)$$

This relation is analysed in Section V where its consequences on hose growth are discussed.

The Lorentzian tends to overestimate the effects of longitudinal velocity spread since the mean of v^2 is divergent. However, in the limit $\Omega_o \to 0$, (68) agrees with the Maxwellian result [employing the distribution (35)] to lowest order in ku and $k\Delta$ if

$$u \simeq \Delta \qquad (69)$$

Numerical comparisons suggest that the real part of the r.h.s. of (68) agrees reasonably well with the Maxwellian weighted results; differences in growth rates are small ($\lesssim$ 40%).

IV.B. Distributed-Mass Model

The distributed-mass model was introduced by Lee (Ref. 7) to incorporate phase-maxing -- associated with the spread in betatron frequency k_β -- into the rigid-beam model. Justification for the model relies on the agreement of its predictions with the results of experiment and particle simulations. In this section, we generalize it to account for longitudinal velocity spread. The procedure is essentially identical to the rigid-beam development in Section IV.A.

Following Reference 7 , we associate with each subset of particles in $(\nu,\nu+d\nu)$ a mass distribution

$$m_\mu = \left(\frac{m}{\mu}\right) \frac{k_s^2}{k_m^2} \tag{70}$$

where μ is a continuous variable with range $0 \leqslant \mu \leqslant 1$, and k_m is the maximum betatron frequency for a particular beam profile, i.e.,

$$k_m^2 \equiv k_\beta^2 \ (r = 0) \tag{71}$$

From (27) and (28), we find

$$k_m^2 = 2\pi \ (1 - \delta_m) \ \frac{J_{bo}(0)}{I_A} \tag{72}$$

which for the Bennett equilibrium gives

$$k_{mB}^2 = \frac{2(1 - \delta_m)}{a^2} \ \frac{I_b}{I_A} \tag{73}$$

We let $\hat{x}_{\mu,\nu}(\xi,z)$ represent the displacement of a disk of particles at (ξ,z) with mass m_μ and velocity $v = v_o + \nu$. The center of current is now given by

$$\langle\langle x(\xi,z)\rangle\rangle \equiv \int_0^1 d\mu \ h(\mu) \int_{-\infty}^{+\infty} d\nu \ F(\nu) \ \hat{x}_{\mu,\nu}(\xi,z) \tag{74}$$

where $h(\mu)\, d\mu$ denotes the fraction of disks with mass m_μ and is normalized to one. Following the arguments of Ref. 7 , we choose

$$h(\mu) = 6\mu\ (1 - \mu) \tag{75}$$

which is zero at $\mu = 0,1$ and peaks at $\mu = 1/2$.

Substituting (70) into (50), we get a new equation of motion for $\hat{X}_{\mu,\nu}$

$$\frac{d^2\hat{X}_{\mu,\nu}}{dz^2} = \mu k_{mB}\ [D(\xi) - \hat{X}_{\mu,\nu}(\xi,z)] \tag{76}$$

and Ampere's relation (55) is modified to

$$D(\xi) + \tau_1 \frac{\partial D}{\partial \xi} = \frac{\langle\langle X(\xi,z)\rangle\rangle}{1 - \delta_m} \tag{77}$$

These two equations along with (74) completely specify the distributed-mass model with longitudinal velocity spread.

The single-mode dispersion equation for the distributed-mass model follows substituting (61) in Eqs. (76) and (77):

$$-i\omega(\Omega_o)\lambda = \int_0^1 d\mu\ 6\mu(1 - \mu) \left\{ \frac{\mu}{(1-\delta_m)} \int_{-\infty}^{+\infty} d\nu \frac{F(\nu)}{\mu-(\Omega_o-k\nu)^2} - 1 \right\} \tag{78}$$

where the dimensionless units now correspond to setting $k_{mB} = 1$ rather than k_{sB} in (63). Note that for zero velocity-spread -- i.e., $F(\nu) = F_c(\nu)$ in (64) -- we recover the distributed-mass dispersion result of Lee with the addition of the current neutralization factor δ_m.

A tractable solution of (78) for finite velocity-spread follows by employing the Lorentzian distribution F_L of (66). Since μ is real and the singular points $\{k\nu_s\}$ (from setting the denominator of the integrand equal to zero) lie in the upper half-plane (for $\mathrm{Im}\,\Omega_o > 0$), we simply replace

kv by $-ik\Delta$. The integration over μ can now be performed to give

$$-i\omega(\Omega_o)\lambda = \frac{1}{(1 - \delta_m)} \{\delta_m + G(\Omega_o + ik\Delta)\} \tag{79}$$

where

$$G(S) \equiv 6S^2 \left[\frac{1}{2} - S^2 + S^2(1 - S^2) \ell n\left(\frac{1 - S^2}{-S^2}\right)\right] \tag{80a}$$

for Im S > 0 and 0 < Re S < 1 .

The branch points of G(S) lie at S = 0,±1 . Since the Ω_o-contour of integration in (60) lies in the upper half-plane, we choose branch lines that extend to $-i\infty$ in the lower half-plane. On the primary sheet for Im S = 0, G(S) is analytically continued into -1 < Re S < 0 and |Re S| > 1 as follows:

$$\ell n\left(\frac{1-S^2}{-S^2}\right) = \begin{cases} +i\pi + \ell n\left|\frac{1-S^2}{S^2}\right| & , \ 0 < \text{Re } S < 1 \\ -i\pi + \ell n\left|\frac{1-S^2}{S^2}\right| & , \ -1 < \text{Re } S < 0 \\ \ell n\left|\frac{1-S^2}{S^2}\right| & , \ |\text{Re } S| > 1 \end{cases} \tag{80b}$$

For Im S ≠ 0, the prescription for determining G(S) is now completely specified.

In the limit $\Omega_o \to 0$, and $\mu \to 0$ (or 1), the Lorentzian distribution in (78) reproduces the Maxwellian result [employing the F_M distribution in (35)] to lowest order if

$$\Delta \simeq u \equiv \langle v^2 \rangle \tag{81}$$

Generally, however, the Lorentzian result (79) by equating Δ with u tends to overestimate the effects of longitudinal velocity-spread -- but by less than 40%. This is more than adequate for our present purposes.

The dispersion equation for the distributed-mass model with finite velocity-spread is now completely specified. Its implications on hose growth are explored in the following section.

V. ANALYSIS OF DISPERSION RELATIONS

V.A. Rigid-Beam

Growth in the beam displacement $\langle X \rangle$ as a function of (ξ,z) is measured by the leading amplitude (60). The growth-phase exponent g for the rigid-beam model follows from (68); with $k_{sB}z \to z$ and $k_{sB}\xi \to \xi$, we have

$$g(\Omega_o) = -i\Omega_o z - i\omega_{RB}(\Omega_o)\lambda \frac{\xi}{\lambda} \tag{82a}$$

$$-i\omega_{RB}(\Omega_o)\lambda = \frac{(\Omega_o + ik\Delta)^2}{[1 - (\Omega_o + ik\Delta)^2]} \tag{82b}$$

where we have set $\zeta_m = 0$ for convenience. For the case $k\Delta = 0$, Figure 1 gives the Im $\omega_{RB} = 0$ contour in complex Ω_o-space; the shaded region corresponds to Im $\omega_{RB} > 0$ -- i.e., where hose growth occurs -- and the broken-line marks the inversion Ω_o-contour of integration for Equation (60). The Ω_o-contour is not permitted to lie entirely in the lower half-plane since there are intrinsic singularities at $\Omega_o = \pm 1$. Since Im Ω_o and/or Im ω_{RB} must be greater than zero over some part of the Ω_o-contour, unstable hose-growth results.

For $k\Delta > 0$, the real axis (Im $\Omega_o = 0$ in Figure 1) shifts up by an amount $k\Delta$. For $k\Delta > .3536$, the unstable region lies entirely in the lower half-plane. Thus, the Ω_o-contour can be taken along the real axis, and hose stability is established. However, the rms-velocity spread u must satisfy the condition

$$ku > .36\ (k_{sB}v_o) \tag{83}$$

which is unrealistic in practice.

For a general understanding of hose growth, we pass the Ω_o inversion contour through a saddle point. The saddle point Ω_{os} satisfies the condition

$$\left(\frac{\partial g}{\partial \Omega_o}\right)_{\Omega_{os}} = 0 = -iz + \frac{2(\Omega_{os} + ik\Delta)}{[1 - (\Omega_{os} + ik\Delta)^2]^2} \frac{\xi}{\lambda} \tag{84}$$

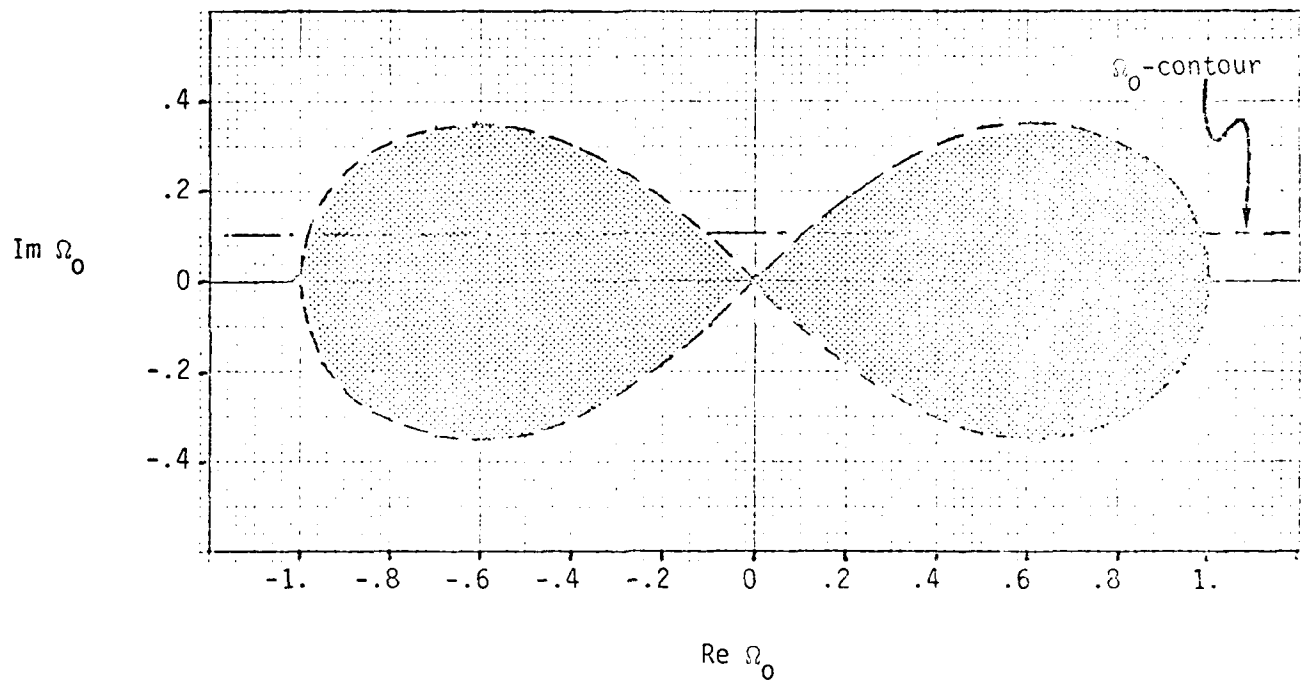

Figure 1. Inversion Contour in Complex Ω_o-Space With $k\Delta = \delta_m = 0$. Shaded Region Designates Im $\omega_{RB} > 0$ for the Dispersion Equation (82b). Finite $k\Delta$ Shifts the Real Axis up by $k\Delta$.

For $z\lambda >> \xi$ and $|1-\Omega_o| << 1$, we find

$$\Omega_{os} \simeq 1 - \frac{1}{2}\left|\frac{\xi}{\lambda z}\right|^{1/2} + i\,\frac{1}{2}\left|\frac{\xi}{\lambda z}\right|^{1/2} - ik\Delta \tag{85}$$

$$g(\Omega_{os}) \simeq - iz + i\left|\frac{z\xi}{\lambda}\right|^{1/2} - zk\Delta + \left|\frac{z\xi}{\lambda}\right|^{1/2} \tag{86}$$

The damping of hose growth due to longitudinal velocity spread is now explicit in the $-zk\Delta$ term of (86).

If we maximize g with respect to z with ξ fixed, we find

$$\left(\frac{\partial g}{\partial z}\right)_\xi = 0 \quad , \quad \Omega_{os} = 0 \tag{87a}$$

$$g_{max} \simeq + \frac{\xi}{4\lambda k\Delta} \tag{87b}$$

This maximum occurs at

$$z_o = \frac{\xi_o}{4\lambda k^2\Delta^2} \tag{87c}$$

Thus, for $\Delta \to 0$, we have unlimited growth for all ξ as a function of z -- i.e., an absolute instability -- which concurs with the rigid-beam result of Reference 7.

For finite velocity spread, the hose displacement amplitude peaks at each ξ-disk with maximum exponent g_{max} and then begins to damp. The maximum displacement occurs at larger z_o with increasing ξ according to (87c). Thus, the hose displacement convects back into the pulse (towards larger ξ) as it grows in amplitude. It is straight-forward to verify that the convection velocity is given by

$$v_c \equiv \frac{\xi_o}{z_o} \simeq 4\lambda k^2\Delta^2 \tag{88}$$

If we allow a maximum displacement gain of 10^3, for example, the maximum pulse length L_p^{max} permitted for hose stable propagation is

$$L_P^{max} \simeq 28\ \lambda\ k\Lambda \tag{89}$$

according to (87b). If we consider a proton beam with

$$E_o - mc^2 = 50\ \text{MeV}$$

$$I_b = 10\ \text{ka} \tag{90a}$$

$$a = .5\ \text{cm}$$

we find $.1 < \lambda < 1$ and $k_{sB} \simeq .051$. Condition (89) then becomes

$$L_P^{max} \lesssim (5.5\ \text{meters})\ \frac{ku}{k_{sB}v_o} \tag{90b}$$

Thus, longitudinal velocity spread alone does <u>not</u> ensure useful hose-stable pulses without imposing severe conditions on the rms velocity-spread.

For $\delta_m > 0$, the growth-phase exponent (82) aquires an additional growth component

$$\frac{+\delta_m}{1 - \delta_m}\ \frac{\xi}{\lambda} \tag{91}$$

which increases the maximum displacement at ξ. Since we are interested in the <u>relative</u> importance of longitudinal velocity-spread on the hose mode, we ignore this plasma return-current effect in the present treatment. Note again that when the denominator in (91) becomes less than .5, the present model begins to loose its validity. For significant current-neutralization, we must take into account the proper radial-profile of conductivity and its dipole perturbation.

V.B. Distributed-Mass Model

The growth-phase exponent for the distributed-mass model is given by (79) with $k_{mB}z \to z$ and $k_{mB}\xi \to \xi$:

$$g(\Omega_o) = -i\Omega_o z + G(\Omega_o + ik\Delta)\frac{\xi}{\lambda} \tag{92}$$

with G defined by (80) and $\delta_m = 0$. For $k\Delta = 0$, the inversion Ω_o-contour for (60a) is plotted in Figure 2. The shaded region corresponds to Re G > 0 or unstable hose growth. The branch cuts are designated by dark, wavy lines extending to $-i\infty$. Since the inversion Ω_o-contour must lie above the branch points $\Omega_o = \pm 1, 0$, it can not be deformed to lie outside the region where either Im $\Omega_o > 0$ or Re G > 0. Therefore, hose instability cannot be avoided.

For finite velocity-spread, the branch points and the Re G > 0 shaded region shift down by an amount $-ik\Delta$. This effect is illustrated in Figure 3 where Re G is plotted as a function of Re Ω_o for various values of $k\Delta$ (with Im $\Omega_o = 0$). With $k\Delta > .183$, the unstable region lies entirely in the lower half-plane and the Ω_o-contour can be taken along the real axis. Thus, we achieve absolute hose stability with an rms velocity-spread u satisfying

$$ku > .183\ (k_{mB}v_o) \tag{93}$$

which is nearly a factor of two less than rigid-beam condition (83) with no k_β-mixing.

We perform a saddle-point analysis on (92) to extract additional information about the hose instability. The saddle point Ω_{os} satisfies the condition

$$\left(\frac{\partial g}{\partial \Omega_o}\right)_{\Omega_{os}} = 0 \tag{94}$$

The values of Ω_{os} have been computed numerically (assuming Im $\Omega_{os} = 0$) and are plotted in Figure 4 (solid-line) as a function of $k\Delta$. Values of the maximum growth-exponent Re $G(\Omega_{os})$ have also been determined. For these

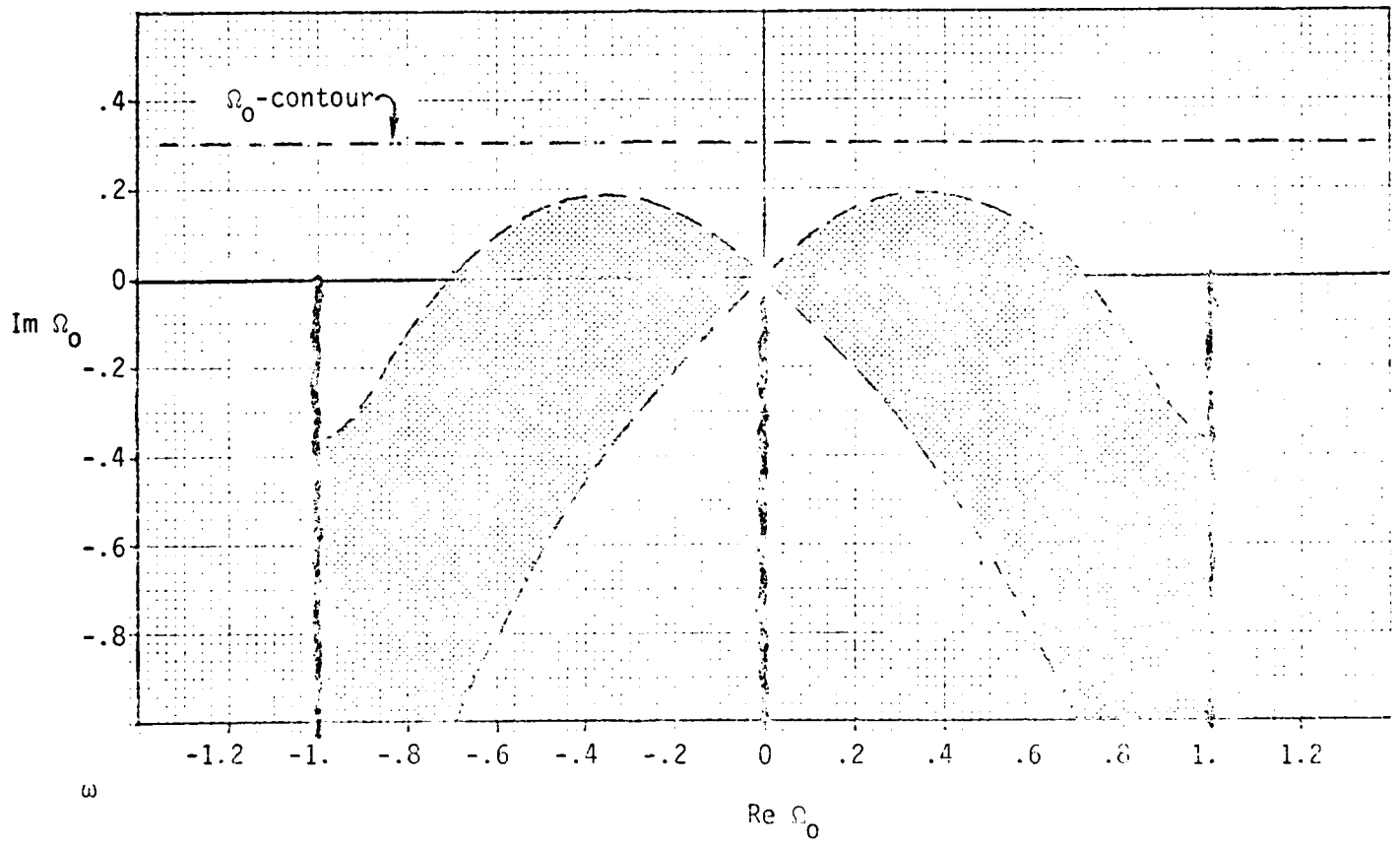

Figure 2. Inversion Contour in Complex Ω_o-Space for Dispersion Equation (79) with $k\Delta = \zeta_m = 0$. Shaded Region Corresponds to Re G > 0 and Dark, Wavy Lines Designate the Branch Cuts.

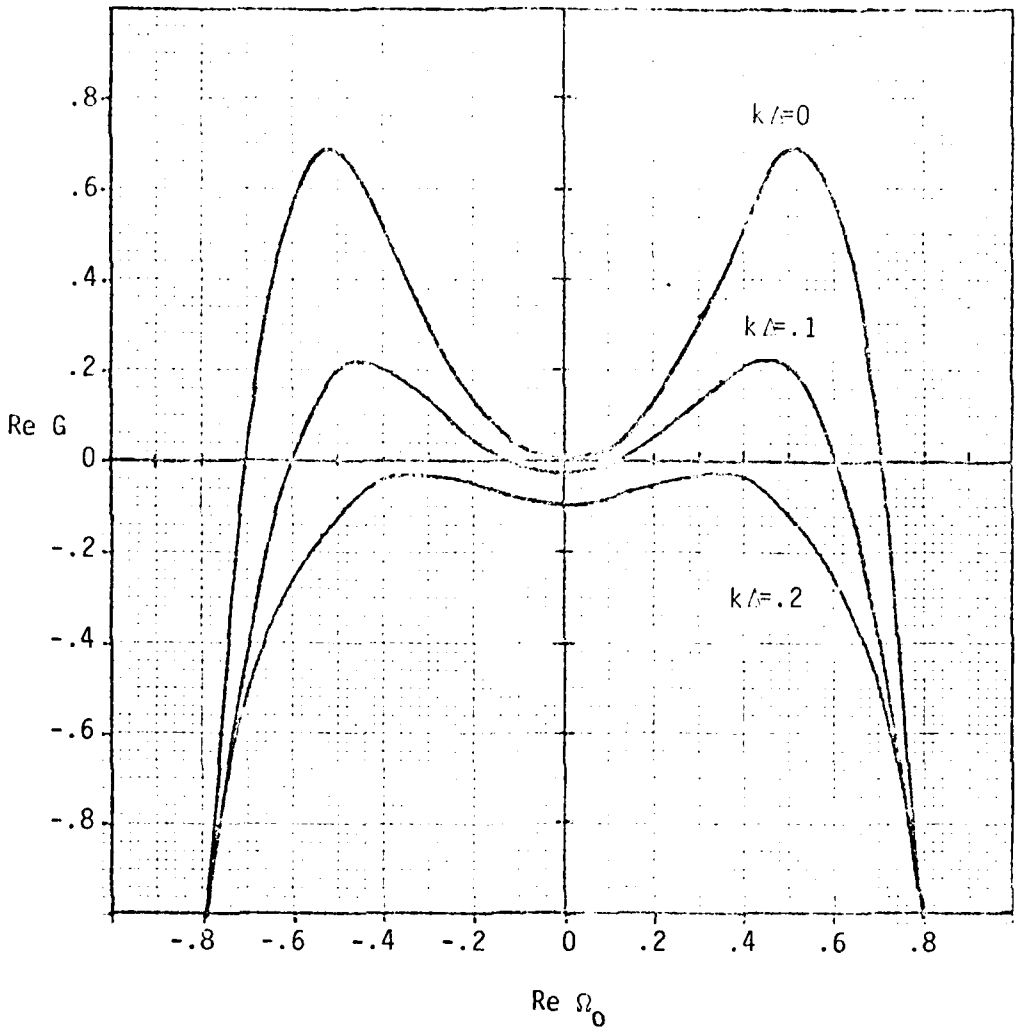

Figure 3. Re G Plotted as a Function of Re Ω_o for Various Values of $k\Delta$ (with Im $\Omega_o = 0$).

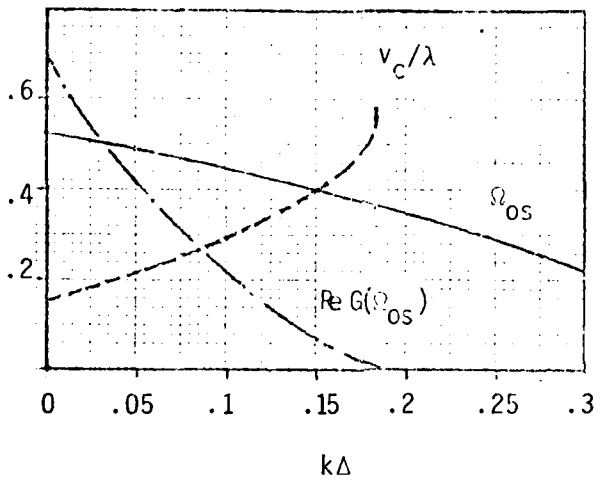

Figure 4. Maximum Growth-Exponent Re $G(\Omega_{os})$, the Saddle Frequency Re Ω_{os} and the Convection Rate v_c/λ Plotted as Functions of $k\Delta$.

values of Ω_{os} and $k\Delta$, we compute the saddle point condition

$$v_c = \frac{-\lambda}{\left[\frac{\partial(\text{Im } G)}{\partial(\text{Re } \Omega_o)}\right]_{\Omega_{os}}} = \frac{\xi_s}{z_s} \tag{95}$$

which represents the rate at which the peak wave-packet convects back towards larger ξ. Values of v_c/λ are also plotted in Figure 4 (dashed-line) in terms of $k\Delta$.

For a given $k\Delta$, we can compute the upper bound on hose growth for a particular ξ-disk by

$$\langle X(\xi)\rangle_{max} \lesssim C\, e^{\text{Re } G(\Omega_{os})\,\frac{\xi}{\lambda}} \tag{96}$$

When the maximum is achieved, the displacement amplitude commences to damp. By expression (95), we see that the hose growth saturates at larger z for increasing ξ. If we allow a maximum gain of 10^3, the pulse length is limited by

$$L_p^{max} \simeq \frac{7\lambda}{\text{Re } G(\Omega_{os})} \tag{97}$$

in units of k_{mB}^{-1}.

For a proton beam with parameters (90a), we have for $k\Delta = .05$, for example, $k_{mB} \simeq .088$ and

$$L_p^{max} \lesssim 2.0 \text{ meters} \quad [\text{for } ku \simeq .05\ (k_{mB}v_o)] \tag{98}$$

which is $\sim$7.3 times longer than that allowed by the rigid-beam model (90b) with no k_β-mixing. For $k\Delta = .1$, we find

$$L_p^{max} \lesssim 3.6 \text{ meters} \quad [\text{for } ku \simeq .1\ (k_{mB}v_o)] \tag{99}$$

To appreciate the effects of longitudinal velocity-spread alone, we compare (98) and (99) to the cold-fluid result ($k\Delta = 0$):

$$L_p^{max} \lesssim 1.2 \text{ meters} \quad [ku = 0] \tag{100}$$

which is a factor of three less than the hose-stable pulse with $ku = .1\ (k_{m\beta}v_o)$.

Note that (98) - (100) are approximate upper-bounds on hose-stable pulse length. Inserting the proper units back into (97) and employing the Bennett results (59) and (73), we find L_p^{max} is proportional to beam current. A decrease in beam current due to longitudinal pulse-spreading would reduce the hose-stable pulse length.

VI. CONCLUSION

In Section V, the distributed-mass model with longitudinal velocity-spread provides approximate conditions for hose-stable propagation. It is useful to compare these results with realistic collective-accelerator projections and with the requirements for longitudinal mass stability.

At the exit-port of the Auto-Resonant Accelerator (ARA), the maximum spread in energy is estimated to be

$$\frac{(\Delta E)^{max}}{E_o} \simeq 6.3\ \beta_o \left| \gamma_o (1 - \beta_o) \frac{m_e}{m} \right|^{1/2} \tag{101}$$

where m_e is the electron mass and m is the ion mass (Ref. 10). This result is due predominantly to longitudinal velocity-spread with ion axial-motion confined by the cyclotron wave potential. For the 50 MeV proton beam (90a), the ARA would produce

$$\frac{(\Delta E)^{max}}{E_o} \simeq .04 \tag{102}$$

The associated rms velocity-spread, according to relation (42), is somewhere in the range

$$.1 \lesssim \frac{u}{v_o} \lesssim .2 \tag{103}$$

Comparing this to predictions (98) and (99), with $k \simeq .5\ k_{mB}$, we would expect a significant increase in hose-stable pulse-length due to longitudinal velocity-spread at the exit-port.

After the beam propagates a distance, some of the longitudinal temperature is converted into transverse temperature by the azimuthal magnetic self-field of the beam. A lower-bound on longitudinal temperature may be found in the dynamics of the longitudinal mass (or bunching) instability. Sloan

et. al. (Ref. 6) have shown that the longitudinal bunching instability in the axi-symmetric monopole mode is Landau damped when

$$\frac{u^2}{v_o^2} \gtrsim \frac{2}{\gamma_o^2 \beta_o} \frac{I_b}{I_A} \tag{104}$$

In fact, this condition is enforced by the instability itself: as the bunching mode grows in amplitude, the rms velocity-spread increases until (104) is satisfied. For the 50 MeV proton beam example, we find

$$\left(\frac{u}{v_o}\right)^{min} \simeq .075 \tag{105}$$

which is reasonably close to the lower bound estimate (103) produced at the exit-port of an ARA. Thus, the bunching instability appears to maintain the longitudinal temperature required for improved hose-stability.

We conclude from these preliminary results that the low-γ light-ion beam may have an advantage over a comparable electron beam insofar as the resistive hose instability is concerned. The degree of advantage (if any) depends, of course, on the amount of velocity-spread the pulse can tolerate -- spreading of the pulse length would reduce its current and decrease its hose-stable length. It has been suggested that a "self-trapped mode" may exist where the beam particles are confined longitudinally by the self-induced electric fields at the front and rear of the pulse (Ref. 5). Verification of this self-trapped state will require a numerical study of the dynamic coupling of longitudinal and transverse degrees of freedom [e.g., a modified LOGAP code (Refs. 1 and 2)].

A more precise quantitative estimate of this hose advantage would also require a comprehensive numerical study of hose dynamics: a self-consistent model with a realistic σ-channel and with the transverse and longitudinal degrees of freedom properly coupled. The latter requirement would permit some of the longitudinal temperature to be converted to the transverse plane by the magnetic self-field. This would result in a new isothermal equilibrium state with a modified beam-current radial-profile.

VII. REFERENCES

1. R.R. Johnston, R.L. Feinstein, *et. al.*, Chapter 2: "Studies in the Propagation of Proton Beams (U)," in SAI Final Report, "Studies of Endo-atmospheric Particle-Beam Technology (U)," SAI-78-201-LJ, (SECRET).

2. R.L. Feinstein and W. Aron, "Studies in the Propagation of Proton Beams (U)," SAI-C-17-PA (15 October 1978) (SECRET).

3. R.R. Johnston, R.L. Feinstein, D.E. Maxwell, E.R. Parkinson, and E.E. Simpson, "Topics in the Response of a Gas to Charged Particle Beams, II (U)," SAI-C-10-PA (15 January 1978) (SECRET).

4. E.P. Lee and R.K. Cooper, Particle Accelerators 7, (1976).

5. M.L. Sloan and M.N. Rosenbluth, "Single Pulse Propagation in a Self-Trapped Mode," ARAC Interim Technical Report, I-ARAC-75-U-10.

6. M.L. Sloan, *et. al.*, ARAC Interim Technical Report, I-ARAC-74-S-17 (SECRET).

7. E.P. Lee, Phys. Fluids 21 (8), 1327 (1978).

8. W.H. Bennett, Phys. Rev. 98, 1584 (1955).

9. E.P. Lee, Phys. Fluids 19, 60 (1976).

10. J.R. Thompson, private communication.

APPENDIX A GEM AND LNGDSP ALGORITHMS

(Excerpts from Section 2.1 of Ref. 1)

In the remainder of this section, we derive the governing equations for low-γ propagation and discuss the numerical methods of solution. The new generalized 2-D algorithm, GEM, which solves axial-symmetric, Maxwell equations in real time, has passed considerable testing. Some results are presented. The longitudinal dispersion algorithm, LNGDSP, is still under development and subject to revision. The radial envelope algorithm is only slightly modified from the version contained in HICAP.

The low-γ propagation code, LOGAP, is intended to model concurrently the root-mean-square (rms) radial envelope and the longitudinal charge distribution of a single-pulse in real time. To make the problem tractable, we impose several simplifying assumptions. First, we ignore the complications of dipole hose instability, and higher order instabilities, by assuming axial symmetry. Second, we impose a modified-Bennett radial profile on the beam current density. This reduces a many-dimensional problem to one involving only the rms-radius and its time derivative. Third, we treat the radial and longitudinal degrees of freedom separately.

We consider a single-pulse of ions moving in the positive $\hat{z}$ direction. At time t=0, the mean velocity $\bar{v}_z(t=0)$ is assumed to be known. At some time $t \geq 0$, we focus our attention on some thin slice of beam cut normal to the direction $\hat{z}$ and moving with some mean velocity $\bar{v}_z(z,t)$. Clearly, at constant t, if $\bar{v}_z$ varies with z, then beam particles will move into neighboring slices, resulting in a shift in $\bar{v}_z$ and charge density.

We monitor the migration of particles numerically by introducing the coordinate transformation

$$\zeta \equiv \beta_o \, ct \tag{A.1}$$

$$\xi \equiv \beta_o \, ct - z$$

where c is the speed of light and $\beta_o c$ is initialized to the mean pulse velocity at t=0. The coordinate ζ is the position of our new reference frame in units of length, and the displacement variable ξ denotes a particular transverse slice of space measured from the origin of the ζ-frame in the negative z direction. The origin ξ=0 is chosen to correspond to the front of the pusle at ζ=t=0. Note that (A.1) is a Galilean transformation - we are still in the laboratory frame of reference.

We transform our governing equations of motion with the following replacements:

$$\frac{\partial}{\partial t} \rightarrow \beta_o c \left(\frac{\partial}{\partial \zeta} + \frac{\partial}{\partial \xi} \right) \tag{A.2}$$

$$\frac{\partial}{\partial z} \rightarrow - \frac{\partial}{\partial \xi}$$

For a fluid description, the Eulerian time derivative transformation is

$$\frac{d}{dt} \rightarrow \beta_o c \frac{\partial}{\partial \zeta} + (\beta_o c - \bar{v}_z) \frac{\partial}{\partial \xi} \tag{A.3}$$

where $\bar{v}_z(\xi,\zeta)$ represents the mean v_z in the slice of beam at (ξ,ζ).

The radial beam current density, J_{br}, and the beam current density in the $\hat{z}$-direction, J_{bz}, are assumed to be known as functions of (r,ξ,ζ). The conductivity σ is generated as a function of (r,ξ,ζ) from the values of E_r, E_z and J_b. For our particular application, we use the simplified beam-induced air conductivity model BEMCID (Ref. 3).

Because of the sensitive dependence of the fields on conductivity, it is necessary to first provide formal solutions to Eq. A.4. We integrate along the "characteristic lines",

$$\xi_A(\zeta) = -\frac{(1-\beta_o)}{\beta_o}(\zeta - \zeta_A) + \xi_A(\zeta_A) \qquad (A.5a)$$

$$\xi_B(\zeta) = +\frac{(1+\beta_o)}{\beta_o}(\zeta - \zeta_B) + \xi_B(\zeta_B) \qquad (A.5b)$$

$$\xi_C(\zeta) = (\zeta - \zeta_C) + \xi_C(\zeta_C) \qquad (A.5c)$$

where

$$\frac{D}{D\zeta_A} = \frac{\partial}{\partial\zeta} - \frac{(1-\beta_o)}{\beta_o}\frac{\partial}{\partial\xi} \qquad (A.6a)$$

$$\frac{D}{D\zeta_B} = \frac{\partial}{\partial\zeta} + \frac{(1+\beta_o)}{\beta_o}\frac{\partial}{\partial\xi} \qquad (A.6b)$$

$$\frac{D}{D\zeta_C} = \frac{\partial}{\partial\zeta} + \frac{\partial}{\partial\xi} \qquad (A.6c)$$

After imposing axial-symmetry and the coordinate transformations (A.1) with (A.2), Maxwell's equations become:

$$\left[\frac{\partial}{\partial\zeta} - \frac{(1-\beta_o)}{\beta_o}\frac{\partial}{\partial\xi}\right](E'_r + E_\phi) - \frac{1}{\beta_o}\frac{\partial}{\partial r}E'_z + \frac{Z_o\sigma}{\beta_o}E'_r + \frac{J_{br}}{\beta_o} = 0 \qquad (A.4a)$$

$$\left[\frac{\partial}{\partial\zeta} + \frac{(1-\beta_o)}{\beta_o}\frac{\partial}{\partial\xi}\right](E'_r - H_\phi) + \frac{1}{\beta_o}\frac{\partial}{\partial r}E'_z + \frac{Z_o\sigma}{\beta_o}E'_r + \frac{J_{br}}{\beta_o} = 0 \qquad (A.4b)$$

$$\left[\frac{\partial}{\partial\zeta} + \frac{\partial}{\partial\xi}\right]E'_z + \frac{Z_o\sigma}{\beta_o}E'_z - \frac{2}{\beta_o}\frac{\partial}{\partial r^2}(rH_\phi) + \frac{J_{bz}}{\beta_o} = 0 \qquad (A.4c)$$

where we have introduced the unit conversion

$$E'_r \equiv \frac{E_r}{Z_o}$$

$$E'_z \equiv \frac{E_z}{Z_o}$$

$$Z_o \equiv \text{free-space impedance}$$

$$= 376.74 \text{ (ohms)}$$

Generally, if

$$\frac{D}{D\zeta_A} F(\zeta) + g(\zeta) F(\zeta) = G(\zeta) \qquad (A.7a)$$

then

$$F(\zeta) = F(\zeta_A)\, e^{-\int_{\zeta_A}^{\zeta} g(\zeta')d\zeta'} + e^{\int_{\zeta_A}^{\zeta} g(\zeta')d\zeta'} \int_{\zeta_A}^{\zeta} G(\zeta')\, e^{\int_{\zeta_A}^{\zeta'} g(\zeta'')d\zeta''} d\zeta' \qquad (A.7b)$$

Hence, the exponential dependence of the fields on conductivity is made explicit.

We refer to the lines (A.5) as characteristics. In Figure A.1, we illustrate our differencing grid and the characteristic lines of integration. If we know the values of the fields at ζ_1 for all (ξ,r), then the values at $\zeta_2 = \zeta_1 + \Delta\zeta$ are found by integrating upward along the characteristics. The relevant difference equations emerge directly from (A.4), using the formal solution (A.7), and are expressed in terms of the two variables (ξ,r). The method of solution is now essentially identical to that of CATHY in Ref. 3. The field values are updated explicitly in ζ and implicitly in the radial dimension.

Our treatment of the (B) and (C) characteristics has two phases (see Figure A.1). First, at the start, when the field profiles are evolving rapidly, the ζ-steps are small and the characteristic lines extend all the way down to the ζ_1-line. After the fields have come to some quasi-equilibrium state, we may increase $\Delta\zeta$ by commencing our (B) and (C) integrations at the previous ξ slice. In other words, E_r^B, H_ϕ^B and E_z^C are interpolated between the old and new values at ξ_{I-1}.

The conductivity $\sigma^2(I-1,J)$ in Figure A.1 is updated according to BMCOND (Ref. 3). We modify its incorporation into GEM, however, by integrating along the proper characteristic, Eq. A.5c, rather than along the line of constant ζ (the "frozen" approximation).

To complete our description of GEM, we provide a prescription for the source terms $J_{bz}(r,\xi,\zeta)$ and $J_{br}(r,\xi,\zeta)$. The radial dependence of both are presumed to be known.

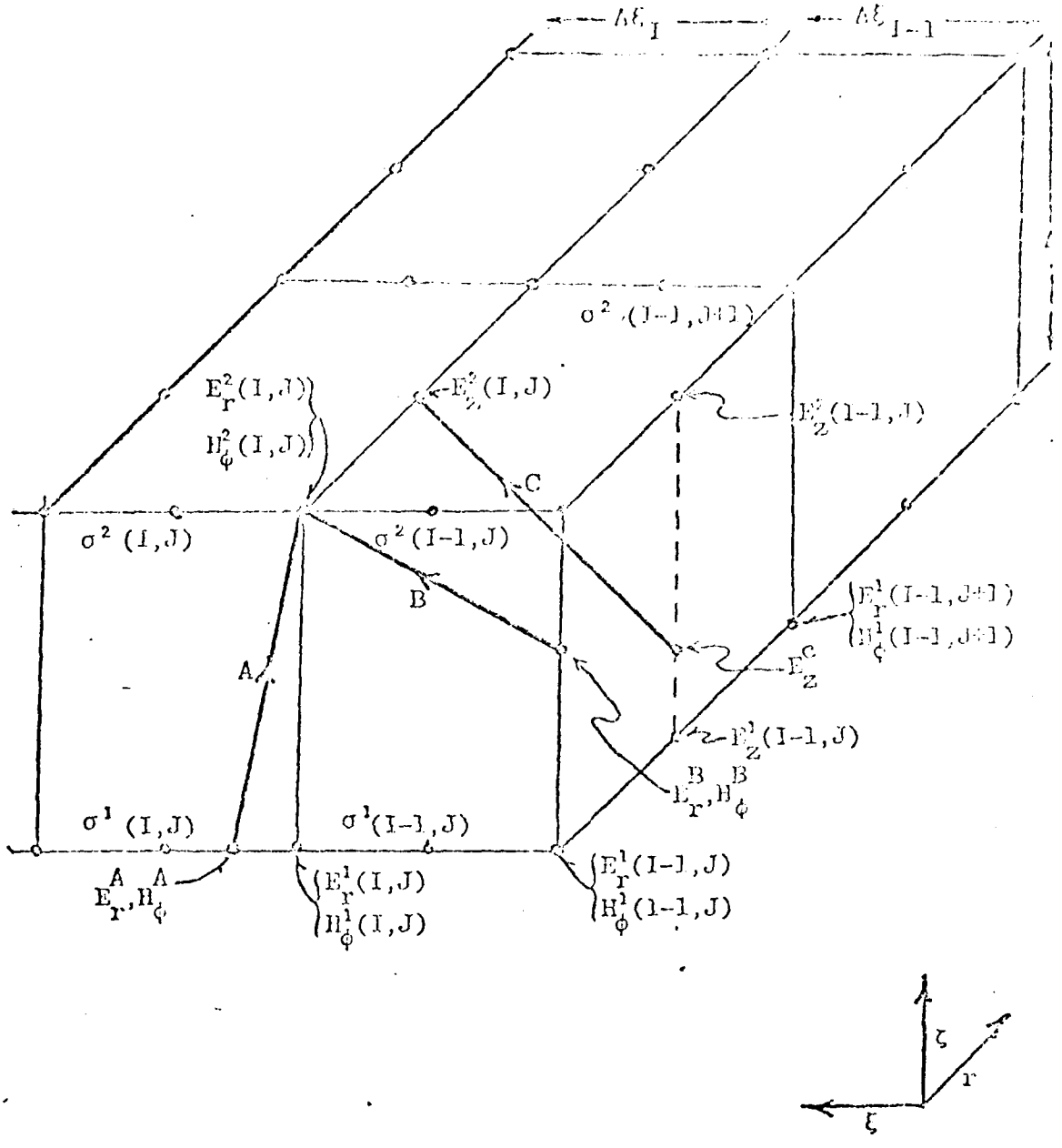
$\Delta\xi_I$
$\Delta\xi_{I-1}$
$\sigma^2(I-1,J+1)$
$E_r^2(I,J)$
$H_\phi^2(I,J)$
$E_z^2(I,J)$
$E_z^2(I-1,J)$
C
$\sigma^2(I,J)$
$\sigma^2(I-1,J)$
B
$E_r^1(I-1,J+1)$
$H_\phi^1(I-1,J+1)$
A
E_z^C
$E_z^1(I-1,J)$
E_r^B, H_ϕ^B
$\sigma^1(I,J)$
$\sigma^1(I-1,J)$
E_r^A, H_ϕ^A
$E_r^1(I,J)$
$H_\phi^1(I,J)$
$E_r^1(I-1,J)$
$H_\phi^1(I-1,J)$
ζ
r
ξ

Figure A.1

For J_{bz}, we impose the modified-Bennett radial profile given by

$$J_{bz}(r,\xi,\zeta) = \frac{K}{\pi R_B^2} N(\xi,\zeta)\,\bar{v}_z(\xi,\zeta)\,\frac{(1 - r^2/R_C^2)^2}{(1 + r^2/R_B^2)^2} \qquad (A.8a)$$

where the radial cutoff is set by the relation

$$R_C = C_R R_B \qquad (A.8b)$$

The Bennett radius R_B satisfies, by definition, the relation

$$R_B \equiv C_B R \qquad (A.8c)$$

with the rms-radius R defined by

$$R \equiv \sqrt{\overline{r^2}} \qquad (A.8d)$$

Once the cutoff coefficient C_R is chosen (usually according to the size and resolution of the radial mesh), the Bennett coefficient C_B follows directly from Eq. A.8c and A.8d. The normalization coefficient K is set by the condition

$$\int_0^{R_C} J_{bz}\, d(\pi r^2) = N(\xi,\zeta)\,\bar{v}_z(\xi,\zeta) \qquad (A.9)$$

and is dependent only on C_R. The beam charge per unit length of pulse, N , is related to the beam current I_b by

$$N(\xi,\zeta) = \frac{I_b(\xi,\zeta)}{\bar{v}_z(\xi,\zeta)} \qquad (A.10)$$

and to the beam charge density ρ_b by

$$N(\xi,\rho) = \int_0^{R_C} \rho_b(r,\xi,\zeta)\, d(\pi r^2) \qquad (A.11)$$

Thus, J_{bz} is completely specified by R, N, and $\bar{v}_z$.

The radial beam current J_{br} is assumed to have the form similar to Eq. A.8a

$$J_{br}(r,\xi,\zeta) = \frac{K}{\pi R_B^2}\, N(\xi,\zeta)\, \bar{v}_r(r,\xi,\zeta)\, \frac{(1-r^2/R_C^2)^2}{(1+r^2/R_B^2)^2} \qquad (A.12a)$$

where we have assumed

$$\bar{v}_r(r,\xi,\zeta) = r\, \frac{\dot{R}(\xi,\zeta)}{R(\xi,\zeta)} \qquad (A.12b)$$

The dot in $\dot{R}$ denotes the total Eulerian time derivative of the rms-radius:

$$\dot{R} \equiv \frac{dR}{dt} \qquad (A.13)$$

The relation (A.12b) is a direct consequence of the self-similar expansion ansatz employed in the derivation of the rms-radial envelope equation (Ref. 3).

The electromagnetic fields in GEM are completely specified as functions of (ξ,ζ) by providing R, $\dot{R}$, N and $\bar{v}_z$. Both R and $\dot{R}$ are solutions of the radial envelope equation of motion derived by Lee and Cooper (Ref. 4). With slight modification, our adaptation for LOGAP is identical to the HIGAP formalism discussed in Ref. 3. We need only to replace the total time derivatives by the transform (A.3). The resulting equations differ from those in HIGAP by the requirement that we integrate along the new characteristic

$$\xi_D(\zeta) = \frac{\beta_o c - \bar{v}_z}{\beta_o c} \quad (\zeta-\zeta_D) + \xi_D(\zeta_D) \qquad (A.14)$$

and that the betatron frequency ω_β (*Eq.* 3.5, *Ref.* 3) be replaced by

$$\omega_\beta^2 \equiv \frac{e}{\gamma m} \quad \frac{(\bar{\beta}\ Z_o H_\phi - E_r)}{r} \qquad (A.15)$$

where $\bar{\beta} \equiv \frac{\bar{v}_z}{c}$, m is the beam particle mass, and e is the electronic charge. The envelope equations are solved simultaneously using 4th order Runge-Kutta.

We must now derive a set of governing equations for the mean charge per unit length N and the mean velocity $\bar{v}_z$. Adopting a fluid description, we introduce the distribution function f where $f(\vec{r}_\perp, z, \vec{p}, t)\, d^2r_\perp\, dz\, d^3p$ is defined to be the number of beam particles with $(\vec{r}_\perp, z, \vec{p})$ in the phase volume $dr_\perp^2\, dz\, dp^3$. The single particle momentum $\vec{p}$ is related to the single particle velocity $\vec{v}$ by

$$\vec{p} = \gamma m \vec{v} \tag{A.16}$$

Because we normalize f to the total number of beam particles in the single pulse, we have

$$n(\vec{r}_\perp, z, t) = \int f\, dp^3 \tag{A.17a}$$

and for the charge and current densities,

$$\rho_b(\vec{r}_\perp, z, t) = e\, n \tag{A.17b}$$

$$\vec{J}_b(\vec{r}_\perp, z, t) = e \int \vec{v}\, f\, dp^3 \tag{A.17c}$$

We define the beam-charge line density by

$$N(z,t) = \int \rho_b\, dr_\perp^2 \tag{A.18}$$

If Q represents some variable of interest, it is convenient to introduce the notation $\langle Q \rangle$ and $\bar{\bar{Q}}$ where

$$\langle Q \rangle \equiv \frac{1}{n} \int Q \, f \, d\vec{p}^3 \qquad (A.19a)$$

and the radial average

$$\bar{\bar{Q}} \equiv \frac{1}{\bar{N}} \int Q \, \rho_b \, d\vec{r}_\perp^2 \qquad (A.19b)$$

In the development to follow, we assume that

$$\bar{\bar{Q}} = \langle \bar{\bar{Q}} \rangle \qquad (A.20)$$

The governing equations of motion can be derived by starting with the Lorentz invariant, collisionless Boltzmann equation:

$$\frac{\partial f}{\partial t} + \frac{\vec{p}}{\gamma m} \cdot \vec{\nabla} f + \vec{F} \cdot \vec{\nabla}_p \, f = 0 \qquad (A.21)$$

where the Lorentz force $\vec{F}$ is just

$$\vec{F} = e\vec{E} + e\vec{v} \times \vec{B} \qquad (A.22)$$

Since we are interested in various momentum moments of A.21, we let $Q(\vec{p})$ represent some function of $\vec{p}$. After multiplying (A.21) by Q and integrating over $\int d\vec{p}^3$, we have

$$\frac{\partial}{\partial t} n \langle Q \rangle + \vec{\nabla} \cdot n \langle Q\vec{v} \rangle - n \langle \vec{F} \cdot \vec{\nabla}_p \rangle Q = 0 \qquad (A.23)$$

where we have used

$$\vec{V}_p \cdot \vec{F} = 0$$

We now multiply Eq. A.23 by the electrostatic charge e and perform the radial integration $\int dr_\perp^2$ to find

$$\frac{\partial}{\partial t} N \langle \bar{\bar{Q}} \rangle + \frac{\partial}{\partial z} N \langle \bar{\bar{Q}} v_z \rangle - N \langle \bar{\bar{\nabla}} \cdot \vec{V}_p Q \rangle = 0 \qquad (A.24)$$

We have imposed axial-symmetry and the condition

$$\lim_{r \to \infty} r^3 \rho_b = 0 \qquad (A.25)$$

Finally, by performing the coordinate transformation (A.2), we have

$$\frac{\partial}{\partial \zeta} N \langle \bar{\bar{Q}} \rangle + \frac{\partial}{\partial \xi} N \left[\langle \bar{\bar{Q}} \rangle - \frac{\langle \bar{\bar{Q}} v_z \rangle}{\beta_o c} \right] = \frac{N}{\beta_o c} \langle \bar{\bar{F}} \cdot V_p Q \rangle \qquad (A.26)$$

To obtain a closed set of equations from Eq. A.26, we proceed as follows. First, we substitute three relations for Q:

$$Q = 1, \; p_z, \text{ and } \gamma \qquad (A.27)$$

where $p_z = \gamma m v_z$. For our particular application, we treat v_z as a functional of $(\gamma, v_\perp)$ and Taylor expand the $\langle \bar{\bar{} } \rangle$ terms about the mean gamma $\bar{\gamma}$, where

$$\gamma \equiv \bar{\gamma} + \delta\gamma \qquad (A.28a)$$

and

$$\langle \bar{\bar{\delta\gamma}} \rangle = 0 \qquad (A.28b)$$

We keep terms only up to second order in the phase dispersion $\delta\gamma$ and ignore the dispersion in the transverse velocity. For example,

$$\bar{v}_z \equiv \langle \dot{z} \rangle$$

$$\approx \hat{v}_z - \theta^2 \left[\frac{3K}{2\bar{\gamma}} + \frac{\bar{\gamma}^3 \hat{v}_z^3}{2c^2} \right] \tag{A.29}$$

where

$$\hat{v}_z \equiv v_z(\bar{\gamma}) = \left[c^2 - \bar{v}_\perp^2 - \frac{c^2}{\bar{\gamma}^2} \right]^{\frac{1}{2}} \tag{A.30}$$

$$\theta^2 \equiv \langle (\delta\gamma)^2 \rangle \tag{A.31}$$

$$K \equiv \frac{c^2}{\bar{\gamma}^3 \hat{v}_z} \tag{A.32}$$

Finally, we assume zero radial correlations between v_z and the electric field E_z, i.e.,

$$\langle \dot{z} E_z \rangle = \langle \dot{z} \rangle \langle E_z \rangle \tag{A.33}$$

This is necessary to complete the separation between the transverse and longitudinal mode. The mean transverse velocity is assumed to be

$$\bar{v}_\perp = \frac{\bar{r}\,\dot{R}}{R} \tag{A.34}$$

in keeping with the self-similar ansatz of the radial envelope equation.

We arrive at the following set of equations:

$$\frac{\partial f_i}{\partial \zeta} + \frac{\partial q_i}{\partial \xi} = h_i \quad , \quad i = (1,2,3) \tag{A.35a}$$

with

$$f_1 \equiv N \quad , q_1 \equiv N \left(1 - \frac{\bar{v}_z}{\beta_o c}\right) \tag{A.35b}$$

$$f_2 \equiv N \overline{\gamma v_z} \quad , q_2 \equiv N \left(\overline{\gamma v_z} - \frac{\overline{\gamma v_z^2}}{\beta_o c} \right) \tag{A.35c}$$

$$f_3 \equiv N \bar{\gamma} \quad , q_3 \equiv N \left(\bar{\gamma} - \overline{\gamma v_z}\right) \tag{A.35d}$$

$$h_1 \equiv 0 \ .$$

$$h_2 \equiv \frac{N}{m\beta_o c} \left\{ \overline{\langle e E_z \rangle} + \overline{\langle e v_r B_\phi \rangle} \right\} \tag{A.35e}$$

$$h_3 \equiv \frac{N}{m\beta_o c^3} \left\{ \bar{v}_z \ \overline{\langle e E_z \rangle} + \overline{\langle e E_r v_r \rangle} \right\} \tag{A.35f}$$

where

$$\overline{\gamma v_z} = \bar{\gamma} \ \bar{v}_z + \theta^2 K \tag{A.36}$$

$$\overline{\gamma v_z^2} = \bar{\gamma} \ \hat{v}_z^2 - \theta^2 \ \hat{v}_z K \tag{A.37}$$

The source terms (A.35e, A.35f) are generated in GEM using

$$\langle \hat{e}\, v_1 E_\zeta \rangle = e^{-\frac{\vec{r}\cdot\vec{E}_\zeta}{R}} \dot{R} \qquad (A.34)$$

and

$$\langle \hat{e}\, v_x E_x \rangle = e^{-\frac{\vec{r}\cdot\vec{E}_x}{R}} \dot{R} \qquad (A.35)$$

The first equation (A.35, i=1) is just the continuity equation for conservation of charge. The momentum transfer is described in the second equation, and energy flow in the third.

APPENDIX B [illegible]

(Excerpts from Ref. 2)

A critical objective [illegible] useful low-γ propagation code [illegible] PM-field algorithm that [illegible] computer time. [illegible] al article G.I. Since [illegible] in LSP, we devote this entire [illegible] stability analysis of CPM. This is particularly important considering its novel approach to differencing and interpolating nearest-neighbor mesh points.

The governing axial-symmetric Maxwell equations and the numerical methods of solution are described in Reference 1 (see Appendix A). There we impose the Galilean transformation

$$\zeta = \beta_o ct$$

$$\xi = \beta_o ct - z \qquad (B.1)$$

$$r = r$$

where ζ measures the distance traveled by our chosen reference frame and the displacement variable, ξ, denotes a particular transverse slice of space measured from the origin of the moving frame, in the negative z direction. The $\beta_o c$ frame velocity is initialized to equal the mean v_z-velocity of the beam particles at t=0. Note that these coordinates are still in the laboratory frame of reference. The resulting difference equations follow directly from Eqs. (A.4) of App. A after imposing the formal solution (A.7). The "characteristic lines" and the interpolation scheme are also described in Appendix A.

We arrive at a set of three equations relating to the field values E_r, E_z, and H_ϕ at the mesh point $(\xi_I, r_J, \zeta_L) \equiv (I,J,L)$ to the field values at (I-1,J,L), (I-1,J+1,L), (I+1,J,L-1), (I,J,L-1), (I-1,J,L-1), (I+1,J+1,L-1), (I,J+1,L-1) and (I-1,J+1,L-1), which are predetermined. The numerical stability of our particular difference scheme can be examined by transforming this set of equations into a dispersion relation, relating the frequency of a Fourier mode on the mesh to particular wave numbers:

$$\omega_\zeta = \omega_\zeta \left(k_\xi, k_r \right)$$

This is achieved by replacing the field variables by their single mode Fourier transform, i.e.,

$$E_z = \hat{E}_z \; e^{i\left[\omega_\zeta L\Delta\zeta - k_\xi I\Delta\xi - k_r J\Delta r\right]}$$

Since we are interested in numerical instabilities, we set all the beam current source terms to zero. We also assume, as we do in GEM, that conductivity remains constant over the characteristic lines of a single mesh interval.

end result is a linear, homogeneous set of equations for the field amplitudes $\hat{E}_z$, $\hat{E}_r$, and $\hat{H}_\phi$. The coefficients of these field amplitudes form a three dimensional matrix M. If the columns of M correspond to $\hat{E}_r$, $\hat{H}_\phi$, and $\hat{E}_z$, respectively, then

$$
\begin{aligned}
M_{11} &= \Omega - A_3((1-C_A)+C_A K) \\
M_{12} &= A_1(\Omega - (1-C_A) - C_A K) \\
M_{13} &= -2\, i \sin(\bar{\lambda}/2)\, A_2(\Omega - (1-C_A) - C_A K) \\
M_{21} &= \Omega - B_3((1-C_B)\,\Omega + C_B)/K \\
M_{22} &= -B_1(\Omega - (1-C_B)\,\Omega/K - C_B/K) \\
M_{23} &= 2\, i \sin(\bar{\lambda}/2)\, B_2(\Omega + (1-C_B)\,\Omega/K + C_B/K) \\
M_{31} &= 0 \\
M_{32} &= i\, C_1 \sin(\bar{\lambda}/2)\,(\Omega\,(-1-(1-C_C)/K) - C_C/K) \\
M_{33} &= \Omega\,(1-C_3(1-C_C)/K) - C_3\, C_C/K
\end{aligned}
\qquad \text{(B.2)}
$$

where

$$
\begin{aligned}
\Omega &\equiv \exp(i\,\omega_\zeta \Delta\zeta) \\
K &\equiv \exp(i\,k_\xi \Delta\xi) \\
\bar{\lambda} &\equiv k_r \Delta r
\end{aligned}
$$

and

$$C_A \equiv \frac{1-\beta_o}{\beta_o} \quad \frac{\Delta r}{\Delta \zeta}$$

$$C_B \equiv \frac{\beta_o}{1+\beta_o} \quad \frac{\Delta z}{\Delta \zeta}$$

$$C_C \equiv \frac{\Delta \zeta}{\Delta \zeta}$$

with

$$A_1 = (1-A_3)/(\bar{\sigma}\ \Delta\zeta/\beta_o)$$

$$A_2 = A_1\ \Delta\zeta\ /(2\beta_o\ \Delta r)$$

$$A_3 = \exp\ (-\ \bar{\sigma}\ \Delta\zeta/\beta_o)$$

$$B_1 = (1-B_3)/(\bar{\sigma}\ \Delta\zeta_B/\beta_o)$$

$$B_2 = B_1\ \Delta\zeta_B/(2\beta_o\ \Delta r)$$

$$B_3 = \exp\ (-\bar{\sigma}\ \Delta\zeta_B/\beta_o)$$

$$C_1 = (1-C_3)\ /\ (\bar{\sigma}\Delta r)$$

$$C_2 = C_1\ \Delta r$$

$$C_3 = \exp\ \left(\frac{-\bar{\sigma}\ \Delta\zeta_C}{\beta_o}\right)$$

and

$$\Delta\zeta_B \equiv C_B \Delta\zeta$$

$$\Delta\zeta_C \equiv C_C \Delta\zeta$$

where we define

$$\bar{\sigma} \equiv Z_o\sigma \quad (cm^{-1})$$

$\sigma \equiv$ conductivity (mho cm^{-1})

$$Z_o \equiv \sqrt{\frac{\mu_o}{\varepsilon_o}} = 376.7 \text{ ohms}$$

The determinant of M must be zero for a nontrivial solution. Thus, we arrive at our dispersion relation, i.e.,

$$\det M = 0$$

The dispersion relation derived from the above matrix is nothing more than a cubic equation for

$$\Omega = e^{j \omega_\zeta \Delta\zeta}$$

Because of its complexity, we employ a numerical root-finding algorithm to solve for

$$| \Omega |$$

in terms of k_ζ, k_r, Δr, $\Delta\xi$, $\Delta\zeta$, σ and β_o. We explore the following variable values:

$$\Delta r = .01 \text{ (cm)}$$

$$\Delta\xi = .2 \text{ (cm)}$$

$$k_\xi \Delta\xi = \pi/4, \quad \pi/2, \quad 3\pi/4, \quad \pi$$

$$k_r \Delta r = \pi/4, \quad \pi/2, \quad 3\pi/4 \quad \pi$$

$$\sigma = 10^{-10}, \; 10^{-6}, \; 10^{-4}, \; 10^{-3}, \; 10^{-2}, \; 10^{-1}, \; 1 \; \left(\frac{\text{mho}}{\text{cm}}\right)$$

$$\beta_o = .5, \; .7, \; .8, \; .9, \; .99, \; .999$$

The time step $\Delta\zeta$ is increased until the stability criteria

$$| \Omega | \; < (1 + 1. \times 10^{-6})$$

is violated. (The root finding algorithm permits a convergence error of 10^{-6}.) Our particular choice for Δr and $\Delta\xi$ is set by the dimensional requirements of our pulse profile. Note that we restrict the range of $k_r \Delta r$ and $k_\xi \Delta\xi$ above, rather than go from 0 to 2π. This is sufficient since the remaining range would give the complex conjugate equation where $|\Omega^*| = |\Omega|$.

We present the results of our research in Figure B.1 by plotting the ratio of $\Delta\zeta_{max}/\Delta\xi$ as a function of β_o for various values of conductivity. We first observe that the maximum allowable $\Delta\zeta_{max}$ for stable field generation satisfies approximately the following relation:

$$\frac{\Delta\zeta_{max}}{\Delta\xi} = \frac{\beta_o}{1-\beta_o} \qquad (B.5)$$

We recognize this to be nothing more than the slope of the forward going "A" characteristic of Eq. (A.5a) in App. A. Thus, we conclude that GEM is unconditionally stable so long as the "A" characteristic does not extend beyond the nearest-neighbor mesh point in ξ.

Second, we note that $\Delta\zeta_{max}$ is effectively insensitive to our choice of conductivity except near $\sigma = 1$(mho/cm). This is to be expected since fields propagate poorly in a highly conducting medium. In other words, numerical errors begin to damp out between mesh points around $\sigma = 1$ (mho/cm).

And finally, we observe that as β_o approaches one, $\Delta\zeta_{max}$ becomes infinite. Thus, in the high-γ limit, we achieve the essential criteria for the high-γ approximation in CATHY.

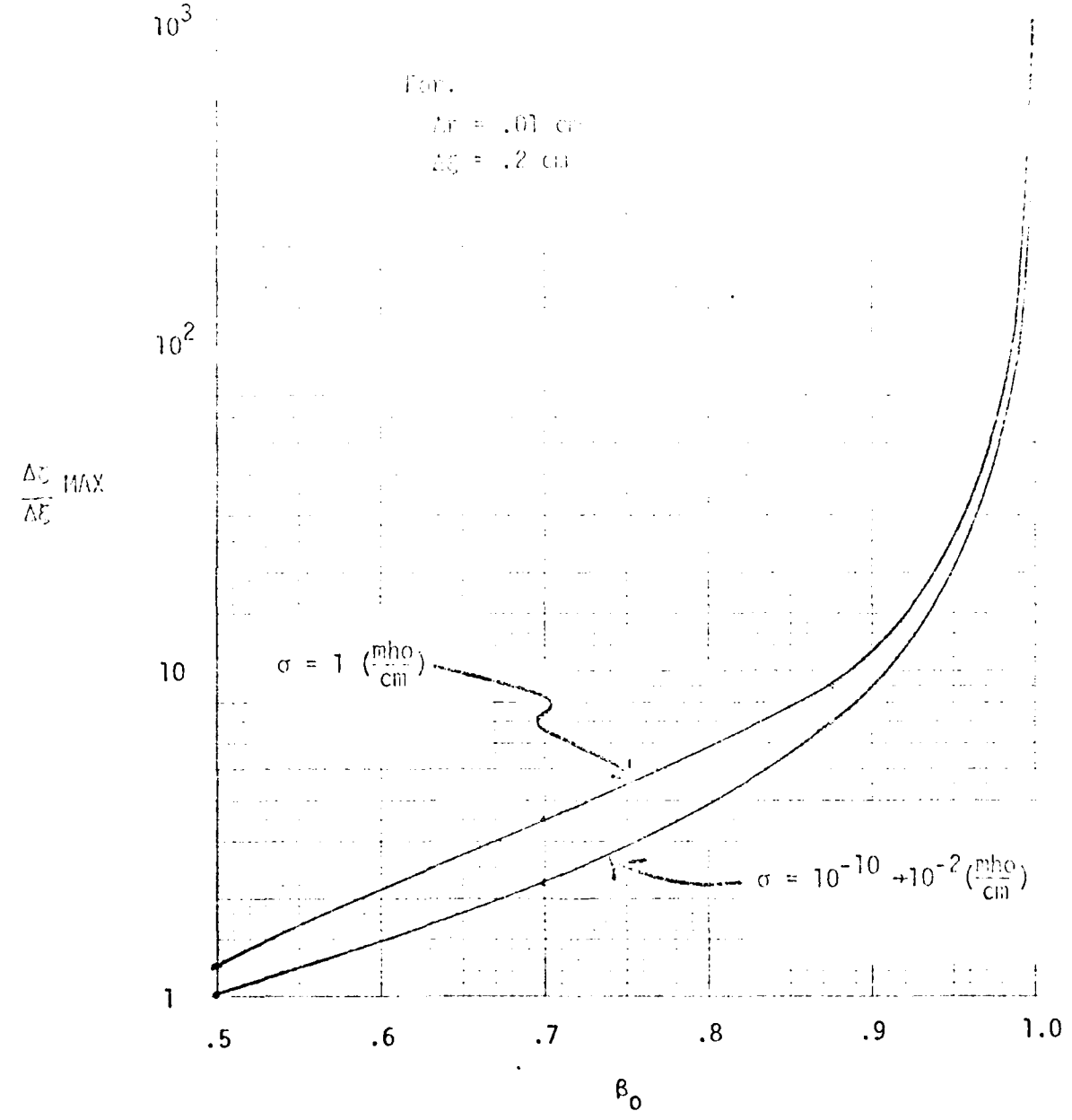

Figure B.1

Maximum Stable $\Delta\zeta$